Spin-orbit torques in the presence of robust interface magnetic state in α-Fe_2O_3/Pt bilayers

T. Z. Zhang,[1,*] K. K. Meng,[1,2,*,†] Y. Wu,[1] J. K. Chen,[1] S. G. Wang,[1] X. G. Xu,[1,‡] and Y. Jiang[1,§]
[1]*School of Materials Science and Engineering, University of Science and Technology Beijing, Beijing 100083, China*
[2]*Department of Applied Physics, The University of Tokyo, Tokyo 113-8656, Japan*

(Received 9 March 2023; revised 6 June 2023; accepted 7 July 2023; published 19 July 2023)

We have investigated the spin-orbit torques (SOTs) driven interfacial magnetization switching in the α-Fe_2O_3/Pt bilayers through pulsed current, DC current and second-harmonic transport measurements. The interfacial magnetic state stems from the combination of the strong spin-orbit coupling of the Pt layer and the magnetic-field-dependent bulk magnetic order of the α-Fe_2O_3 layer. The fieldlike SOT is demonstrated to be the dominated role and has shown a nonlinear relationship with the current amplitude and the magnetic field, indicating the involvement of the interfacial magnetic order. The vast richness of magnetic textures based on the antiferromagnetic insulator/heavy metal bilayers offers a fascinating playground for the investigation of spin transport. Our paper could provide the basis for a deeper understanding of the underlying mechanisms.

DOI: 10.1103/PhysRevB.108.014422

Interfacial effects have long played a crucial role in the development of underlying scientific principles and in the many technologies in which magnetism plays a critical role. The combination of bulk magnetic structure and the strong spin-orbit coupling (SOC) in the magnetic materials/heavy metals (HM) bilayers may enable novel interfacial magnetic and transport properties [1]. For example, the interfaces will promote possible novel interfacial magnetic configurations through the strong SOC [2–4]. Many excitements in the field of interfacial properties arises from the recently developed understanding that interfaces can enable particularly efficient modulation and/or generation of spin currents and, hence, spin torques, which can be used to manipulate the magnetization [5]. One of the key developments in investigating and understanding the interfacial magnetic state and transport properties is the notion of spin-orbit torques (SOT). Quite recently, the SOT-induced Néel vector switching in the antiferromagnetic insulators (AFI)/HM bilayers has raised wide interest since the antiferromagnets are anticipated to replace their ferromagnetic counterparts as the active spin-dependent element in spintronic devices [3,6–20]. Furthermore, using insulating antiferromagnets is more beneficial for investigating spin transmission, potential low-power memory, and logic applications, such as electric-field switching of multiferroic antiferromagnets. If a charge current is applied within the AFI/HM bilayers plane, the bulk spin Hall effect [21] (SHE) and/or inverse spin galvanic effect [22] (iSGE) generates a pure spin current flowing vertically toward the antiferromagnetic insulator. Then, this spin current will apply torques to the AFI via transfer of spin angular momentum, and the magnetic order can be driven. Generally, in bilayers of ferromagnets with HMs, the SOT contains dampinglike and fieldlike terms, which stem from both bulk and interfacial SOCs [23]. In contrast, although the interaction between spin current and antiferromagnetic structures is of great interest for manipulating the magnetic order, an understanding of SOT in the presence of interfacial magnetic state in AFI/HM bilayers, accounting for spin-orbit effects, is so far lacking.

The α-Fe_2O_3 film is a common antiferromagnetic insulator [24,25] in which the spin of Fe^{3+} ions are ordered ferromagnetically on the (0001) plane and follow the "$+\ -\ -\ +$" sequence vertical to the (0001) plane above the Morin transition temperature [26] with a weak ferromagnetism due to the weak Dzyaloshinskii-Moriya interaction [27]. Previously, we have investigated the temperature-dependent spin Hall magnetoresistance (SMR) in the α-Fe_2O_3/Pt bilayers [28] in which the α-Fe_2O_3 has a large out-of-plane magnetic component. The modulated spin transport behaviors have been ascribed to the competition between the modulated interface magnetic texture and the antiferromagnetic bulk state. In this paper, we have further investigated the SOT-driven interfacial magnetization switching in the α-Fe_2O_3/Pt bilayers. A long-range order of the interfacial magnetic state should be formed due to the combination of the SOC of the Pt layer and the magnetic-field-dependent bulk magnetic order of the α-Fe_2O_3 layer. The interaction between the spin current and the interfacial magnetic vector determines the SOT-driven interfacial magnetization movement. Detailed pulsed current, DC current and second-harmonic transport measurements have been carried out. The fieldlike SOT is demonstrated to be the dominated role and has shown a nonlinear relationship with the current amplitude and the magnetic field, indicating the involvement of the interfacial magnetic order.

The preparation and structure characterization of the Al_2O_3 $(11\bar{2}0)$ (Sub.)/α-Fe_2O_3 (15 nm)/Pt (3 nm) films have been described in our previous work [28]. The crystal structure and spin distribution are illustrated in Fig. 1(a). The easy magnetic plane transits from the in-plane to the out-of-plane with a large

*These authors contributed equally to this work.
†kkmeng@ustb.edu.cn
‡xgxu@ustb.edu.cn
§yjiang@ustb.edu.cn

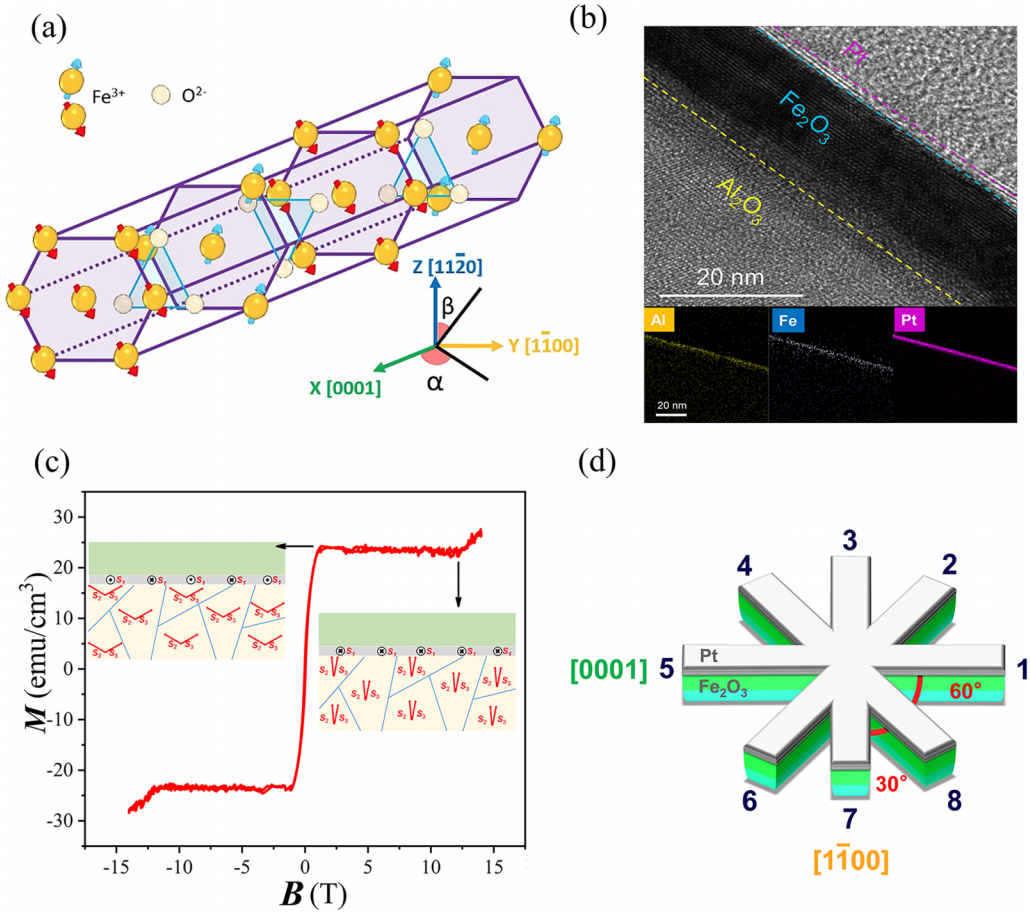

FIG. 1. (a) The magnetic structure of the α-Fe_2O_3 layer that deposited on the Al_2O_3 (11$\bar{2}$0) substrate and the schematic of the corresponding coordinate systems. (b) The transmission electron microscopy of the α-Fe_2O_3/Pt bilayers. (c) The perpendicular magnetic-field-dependent magnetization of the α-Fe_2O_3/Pt bilayers at room temperature. (d) Schematic of the eight-terminals Hall devices.

magnetic component. Here, the high film structure quality has further been confirmed through cross-sectional TEM as shown in Fig. 1(b), which demonstrates explicitly the sharp interface and confirms the preparation of continuous Fe_2O_3 films. The results of the atomic force microscopy and the scanning electron microscopy measurements for the Fe_2O_3 (15 nm)/Pt (3 nm) films are shown in the Supplemental Mateial Figure S1 to confirm that the films are continuous and uniform [29]. The surface roughness is about 0.407 nm, and there are no obvious pinholes or missing areas of the surface, indicating that the Pt film is also continuous. Figure 1(c) shows the ***M-H*** curve with scanning the perpendicular magnetic field at room temperature using vibrating sample magnetometer. One can find that the α-Fe_2O_3 film has undertaken two magnetic transition processes. As increasing the magnetic field to $\sim$ 0.2 T, the spin flip for the α-Fe_2O_3 film has been found [25]. In this case, the net magnetic moment is parallel to the external magnetic field. However, the magnetic moments still maintain an antiferromagnetic arrangement, and the net magnetization remains constant to 12 T. The second transition happens as further increasing the magnetic field (>12 T). In this case, the antiferromagnetic coupling has further been gradually broken as the increasing field. The magnetic moments rotate in the direction of the magnetic field. During this transition process, the system undergoes multiple metastable transitions, so the remanent magnetization has some slight decrease. There is still a small inclination angle between the magnetic moments. As further increasing the magnetic field, the tilt angle becomes smaller, and the net magnetization increases. One of the possible configurations, which will evolve under a perpendicular magnetic field is shown in the inset graph of Fig. 1(c) in which the interfacial magnetic vector $\boldsymbol{m}_n$ can be formed by the interactions of the vector spins $\boldsymbol{S}_1$, $\boldsymbol{S}_2$ and $\boldsymbol{S}_3$. We have further performed the in-plane ***M-H*** measurement as illustrated in Fig. S2 of the Supplemental Material [29], which has shown a similar magnetic transition characteristic.

The transport of the α-Fe_2O_3/Pt bilayers should depend on the magnetic structures of the α-Fe_2O_3 layer, and the interface properties should play the dominated role [28,30]. In our previous work, we have demonstrated the competition between the modulated magnetic state at the α-Fe_2O_3/Pt interface and the bulk antiferromagnetic state of the α-Fe_2O_3 layer, resulting in a special temperature-dependent transport behaviors [28]. In this paper, we have patterned the Al_2O_3 (11$\bar{2}$0)/ α-Fe_2O_3/Pt films into the eight-terminals Hall devices as illustrated in Fig. 1(d) where the length and width of each terminal is 100 and 10 μm respectively. All the transport measurements have been performed in physical property measurement system. Fig. 2(a) shows the variation of Hall resistance R_s^H versus current pulse counts of $\boldsymbol{I}_w$ under zero

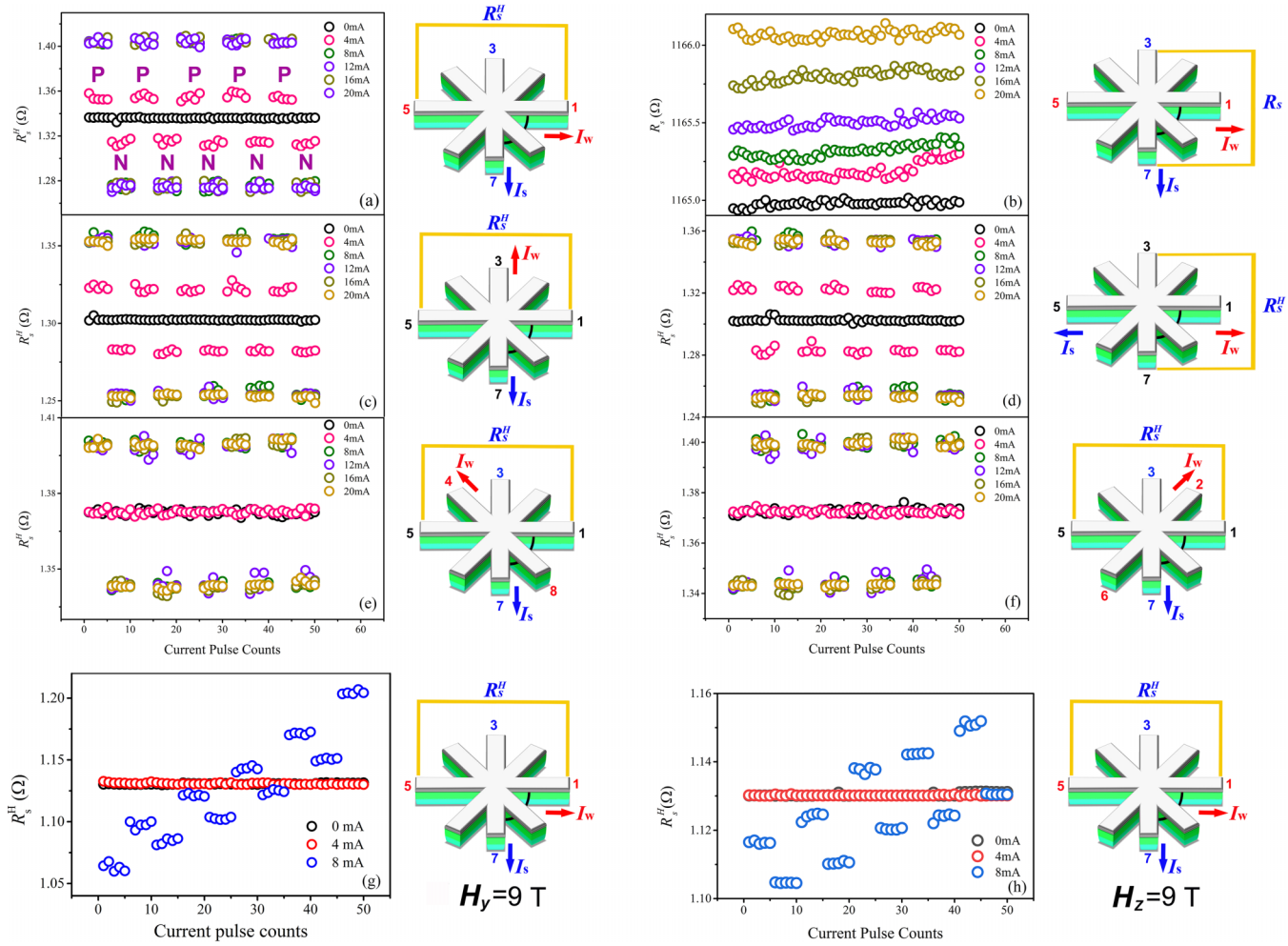

FIG. 2. The variation of Hall resistance R_s^H of the α-Fe_2O_3/Pt bilayers versus current pulse counts of $\boldsymbol{I}_\mathbf{w}$ under zero magnetic-fields (a)–(f) in-plane magnetic fields of 9 T (g) and out-of-plane magnetic fields of 9 T (f). The experimental schematics are shown in the right panels.

magnetic field, and the experimental schematic is shown in the right panel. We have first applied the writing pulsed current $\boldsymbol{I}_\mathbf{w}$ with pulse width 1 ms and varying amplitude along the terminal direction $5 \rightarrow 1$. With a delay of 10 min for thermal relaxation, the Hall resistance R_s^H was measured with applying sensing DC current $\boldsymbol{I}_\mathrm{s}$ of 0.1 mA along the terminal direction $3 \rightarrow 7$. Then, the next same measurement was performed. This kind of process is denoted as "*P*" as shown in Fig. 2(a). After five successive repetitions, the direction of $\boldsymbol{I}_\mathbf{w}$ was switched from terminal $5 \rightarrow 1$ to $1 \rightarrow 5$. The Hall resistance R_s^H was measured after a same 10-min delay with applying sensing DC current $\boldsymbol{I}_\mathrm{s}$ along terminal $3 \rightarrow 7$, and the process is denoted as "*N*." Finally, another five successive repetitions were conducted. Therefore, ten values of R_s^H have been recorded for one test period $(P + N)$, and we have carried out five periods and received 50 values for each fixed amplitude of $\boldsymbol{I}_\mathbf{w}$. With increasing the amplitude of $\boldsymbol{I}_\mathbf{w}$ from 0 to 8 mA, one can find evident changes in R_s^H. However, the changes are found to be saturated with furthering increasing the amplitude of $\boldsymbol{I}_\mathbf{w}$ from 8 to 20 mA. Here, we want to note that the above characteristics are robust even the delay time was changed from 60 to 360 s as shown in Supplemental Material Fig. S3 [29], which indicates the negligible thermal effect. It can be further demonstrated by the results shown in Fig. 2(b) in which the longitudinal resistance R_s was recorded with the same measurement method. It is found tha as increasing the amplitude of $\boldsymbol{I}_\mathbf{w}$, the thermal effect seems to be larger, resulting in the enhancement of R_s. As stated above, after applying the writing pulsed current, there is a delay of 10 min for thermal relaxation. As the pulsed current intensity increases, the sample temperature could even be slightly different after 10 min, which will result in different longitudinal resistance. However, the longitudinal resistance does not show a quadratic relationship with the pulsed current intensity [31]. Therefore, there should be another more dominated mechanism to determine the variation of the longitudinal resistances. As discussed in our previous work [28], we have found the positive field-dependent longitudinal magnetoresistance (FDMR) at room temperature for both in-plane $(\boldsymbol{B}\|\boldsymbol{I})$ and out-of-plane $(\boldsymbol{B}\perp\boldsymbol{I})$ cases. Furthermore, the FDMR curve is an even function on the magnetic field, whereas, the Hall resistance is an odd function. Therefore, as switching the direction of $\boldsymbol{I}_\mathbf{w}$, the variation of the longitudinal resistance does not show a steplike characteristic. As increasing

the amplitude of $\boldsymbol{I}_{\mathbf{w}}$, the longitudinal resistance will increase, corresponding to the positive FDMR at room temprature as discussed in our previous work [28].

We have also performed the switching measurements and recorded the Hall resistance R_s^H when both $\boldsymbol{I}_{\mathbf{w}}$ and $\boldsymbol{I}_{\mathrm{s}}$ were applied along the same terminal directions, such as $3 \leftrightarrow 7$ and $1 \leftrightarrow 5$, and corresponding results are shown in Figs. 2(c) and 2(d) respectively. All the variation characteristics are evident and similar with the results shown in Fig. 2(a). However, as the direction of $\boldsymbol{I}_{\mathrm{s}}$ is fixed along terminal $3 \rightarrow 7$, whereas, the $\boldsymbol{I}_{\mathbf{w}}$ is applied along $4 \leftrightarrow 8$ and $2 \leftrightarrow 6$, the variations of Hall resistance R_s^H have not shown steplike characteristics under $|\boldsymbol{I}_{\mathbf{w}}| = 4$ mA as shown in Figs. 2(e) and 2(f), respectively. The features could be induced by the relatively larger magnetic anisotropy energy in these planes as compared with the (0001) and $(1\bar{1}00)$ planes, which need stronger SOT to switch the Fe^{3+} sublattice magnetic moments. On the other hand, the signals from the Fe^{3+} sublattice magnetic moments components that lay on the in-plane and out-of-plane plane may have opposite variations and compensate each other. Meanwhile, an opposite resistance states has been found in Fig. 2(f), which is ascribed to the opposite direction between the initial writing current and the sensing current.

Generally, the sawtooth switching in AFI/HM bilayers is due to an artifact of Pt, whereas, the actual SOT induced antiferromagnetic switching is steplike [31–38]. Cheng *et al.* have attributed it to the improved stability of the 2-nm-thick Pt layer after the annealing by a high pulse current density 9×10^7 A/cm^2 [36]. However, Zhang *et al.* have conditioned the samples with the current density of 2.5×10^7 A/cm^2 [38]. Furthermore, the authors have stated that the current-induced annealing can change magnetic anisotropy other than the stability of the 5-nm-thick Pt layer. It seems that the annealing current is much different. It could depend on the different preparation method, the quality of the Pt layer, and/or the equipment. In our paper, we have prepared the α-Fe_2O_3 layer using pulsed laser deposition, and the 3-nm-thick Pt layer was deposited *in situ* with magnetron sputtering. The width of each terminal is 10 μm, so the current density for $I_{\mathbf{w}} = 4$ mA is 1.3×10^7 A/cm^2. As shown in Fig. 2, in general, more evident variations of the Hall resistance happen as $\boldsymbol{I}_{\mathbf{w}} \geqslant 4$ mA. Therefore, there could be the current-induced annealing effect, but we have not found the changing process from the sawtooth switching to the steplike switching. Furthermore, the variation of the Hall resistance has found to be constant as increasing the pulsed current $\boldsymbol{I}_{\mathbf{w}}$ from 8 to 20 mA, which indicates the negligible thermal effect induced by the pulsed current. Therefore, the steplike Hall signals should not be generated by the electrothermal effect [36–38]. The evident variations of the Hall signals in the current range in our paper should mainly stem from the SOT-induced magnetization switching.

On the other hand, the Hall effect in the α-Fe_2O_3/Pt bilayers is determined by both the magnetic field and the magnetization, and we have further measured the Hall effect of the α-Fe_2O_3/Pt bilayers in the perpendicular magnetic field ranged from −9 T to 9 T as well as the planner Hall effect under the in-plane magnetic field of 9 T. The results are shown in Fig. S4 of the Supplemental Material [29]. We have found that as the device was applied to the in-plane magnetic field, the change in the Hall resistance ΔR_{xy} is much smaller than the values that were shown in the Figs. 2(a)–2(f). In contrast, the change in the Hall resistance ΔR_{xy} were much larger and were comparable with the values in Figs. 2(a)–2(f). The interfacial magnetic moment could have both the in-plane and the out-of-plane components for which we have given the schematic in Fig. S5 of the Supplemental Material [29]. To further separate the contributions of the interfacial magnetic state and the bulk antiferromagnetic structures of the α-Fe_2O_3 film, we have performed the switching measurements under the in-plane $\boldsymbol{B}_{\mathbf{Y}}$ and out-of-plane magnetic-field $\boldsymbol{B}_{\mathbf{Z}}$ 9 T as shown in Figs. 2(g) and 2(h), respectively. One can find that the Hall resistances R_s^H in both of the two cases evolve into a gradual increase of high-low resistance signal alternately as carrying forward the measurement periods. On the other hand, the relative difference between high and low values becomes much smaller than the case of zero magnetic field, which could be ascribed to the progressive evolvement of the interface magnetic state driven by the spin current and/or the magnetothermal effect.

To clarify the current-dependent transport behaviors, we have also carried out the angular-dependent longitudinal magnetoresistance (ADMR) (ADMR $= \frac{\Delta\rho_L}{\rho_0} = \frac{\rho_L(B)-\rho_L(0)}{\rho_L(0)}$) measurements at room temperature with varying DC current. Fig. 3(a) and 3(b) show the SMR with rotating the magnetic field of 9 T applied in the *Y-Z* plane and varying the current from 0.5 to 3 mA and 4 to 7 mA respectively [(β denotes the angle related to *Z* axis as shown in Fig. 1(a)]. One can find that the peaks at 90 ° and 270 ° gradually shift to 0 ° and 360 ° as increasing the current from 0.5 to 3 mA since the SOT generated by the adjacent heavy metal compensated the tilting tendency from the applied magnetic field. Further increasing the current to 4 mA has instantaneously changed the SMR signals configuration from the *M*-shaped antiferromagnetic configuration to the *W*-shaped ferromagnetic one. It further confirmed the SOT has induced the switching of interface magnetic structure as well as the Néel vector in α-Fe_2O_3/Pt bilayers as discussed in previous report. We also performed the SMR measurement with varying current in smaller range as shown in the Supplemental Material Fig. S6 [29] to exclude the possible electrothermal effect. Figures 3(c) and 3(d) illustrate the $\frac{\Delta\rho_L}{\rho_0}$ with rotating the magnetic field of 9 T on the *X-Y* plane and varying the current from 0.5 to 3 mA and 4 to 7 mA, respectively [α denotes the angle related to the *X* axis as shown in Fig. 1(a)]. It is found that as increasing the current, the $\frac{\Delta\rho_L}{\rho_0}$ signal featured a 45 °-shift characteristic, which confirmed the existence of SOT under the in-plane large magnetic field. It also further reveals that the SOT-induced spin flop in our prepared α-Fe_2O_3/Pt bilayers, which can be characterized as the steplike variations of the Hall resistance R_s^H as shown in Fig. 2, should have both the in-plane and the our-of-plane components. It could also explain why there is no evident change in R_s^H when $|\boldsymbol{I}_{\mathbf{w}}| = 4$ mA as shown in Figs. 2(g) and 2(h) since the switching of the in-plane and the our-of-plane components have compensated with each other.

To further improve that the interfacial magnetic order can be driven by the spin current, we then performed the harmonic resistance measurement. A lock-in technique was employed to record the harmonic resistances with applying an AC current

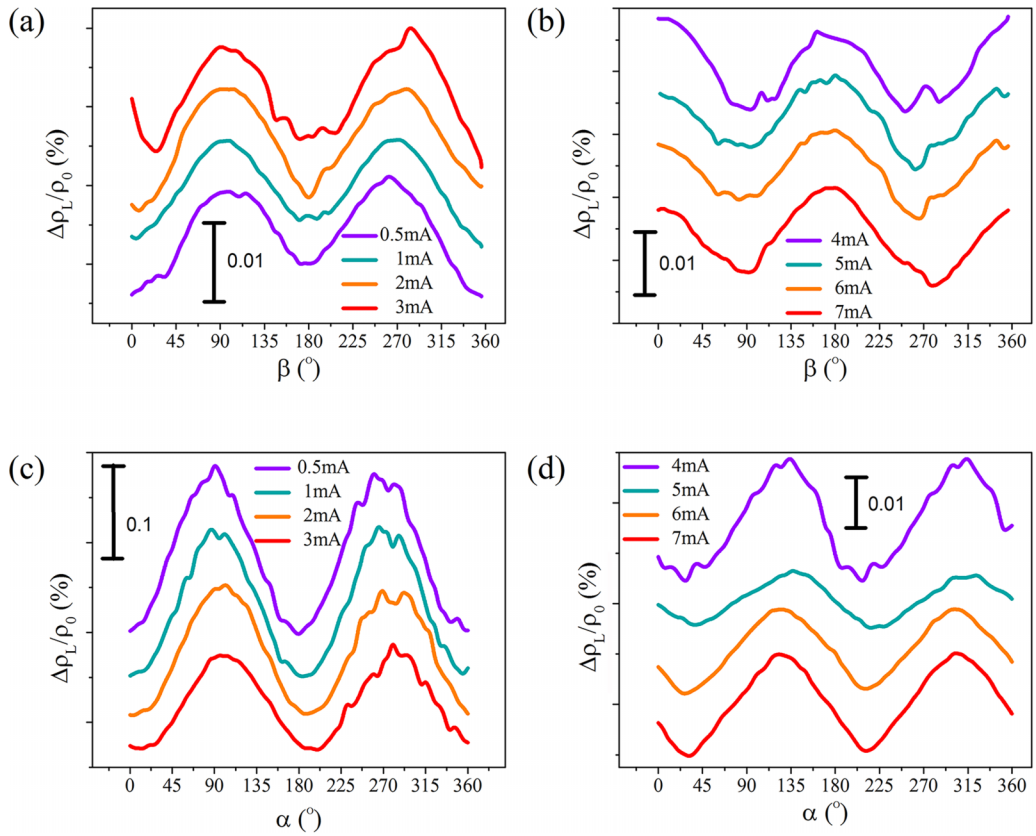

FIG. 3. Angular-dependent longitudinal magnetoresistance of the α-Fe_2O_3/Pt bilayers at room temperature with varying applied DC current.

$I_{ac} = I \sin\omega t$ of frequency 13 Hz. Figs. 4(a) and 4(b) show the transverse second-harmonic resistances ($\Delta R_{xy}^{2\omega}$) with rotating the magnetic field on the X-Y plane with varying the amplitude of current and magnetic field at room temperature, respectively. It is found that the results can be well fitted by [39–44]

$$\Delta R_{xy}^{2\omega} = \left(R_{xy}^{\mathrm{D}} + R_{xy}^{\nabla T}\right)\cos\alpha + \left(R_{xy}^{\mathrm{F}} + R_{xy}^{\mathrm{Oe}}\right)(2\cos^3\alpha - \cos\alpha) \quad (1)$$

where the Oersted (Oe) (R_{xy}^{Oe}) and fieldlike SOT (R_{xy}^{F}) contribute in the form of $(2\cos^3\alpha - \cos\alpha)$, and, whereas, the contribution from the dampinglike SOT (R_{xy}^{D}) and magnetothermal effects ($R_{xy}^{\nabla T}$) take the form of $\cos\alpha$. The inset graph of Fig. 4(a) shows the example of fitting as $I = 8$ mA. A more detailed discussion about the contribution from the magnetothermal effects to the transverse second-harmonic resistances have been shown in the Supplemental Material [29] and Refs. [45–49]. It seems that R_{xy}^{D} cannot be separated from $R_{xy}^{\nabla T}$ precisely, which is the same for R_{xy}^{F} and R_{xy}^{Oe}. However, it should be noted that, even there are magnetothermal and Oersted contributions, the sign of $R_{xy}^{\nabla T}$ and R_{xy}^{Oe} should not change as varying current and magnetic field. Then, we have extracted the $(R_{xy}^{\mathrm{D}} + R_{xy}^{\nabla T})$ and the $(R_{xy}^{\mathrm{F}} + R_{xy}^{\mathrm{Oe}})$ terms separately and plotted them versus the amplitude of current and magnetic field as shown in Figs. 4(c) and 4(d), respectively. It is found that, under relatively small current and magnetic field, both the two terms are negative, which should be determined by the combination of bulk α-Fe_2O_3 and the interface magnetic state. Considering the spin-flip field of bulk α-Fe_2O_3 is very small (~ 0.1 T), both damping and fieldlike torques, which are R_{xy}^{D} and R_{xy}^{F} in Eq. (1) should be suppressed under as $\boldsymbol{H} > 4$ T. Therefore, the bulk α-Fe_2O_3 only contributes $R_{xy}^{\nabla T}$ and R_{xy}^{F} into the results shown in Figs. 4(c) and 4(d) respectively. On the other hand, according to the data where $\boldsymbol{I} = 2$ mA and $\boldsymbol{H} = 9$ T as shown in Fig. 4(a), one can also confirm that $R_{xy}^{\nabla T}$ and R_{xy}^{F} from bulk α-Fe_2O_3 should be negative and the amplitude are all very small. As increasing the current [Fig. 4(c)] or the magnetic field [Fig. 4(d)], the amplitude of $(R_{xy}^{\mathrm{D}} + R_{xy}^{\nabla T})$ has decreased. More pronouncedly, the signs of $(R_{xy}^{\mathrm{F}} + R_{xy}^{\mathrm{Oe}})$ have changed from negative to positive, and the values increase with enhancing $\boldsymbol{I}$ and $\boldsymbol{H}$. In this case, $\Delta R_{xy}^{2\omega}$ should be mainly determined by the fieldlike torques as the spin current was applied to the interfacial magnetic state, which should involve the magnetic field as discussed above. As increasing the magnetic field, $\Delta R_{xy}^{2\omega\prime}$s have shown a nonlinear relationship with the magnetic field due to the evolvement of the interfacial magnetic order. The $\Delta R_{xy}^{2\omega}$ measurements with varying in-plane magnetic field and scanning the magnetic field along X and Z directions are shown in Supplemental Material Fig. S7 [29].

The interaction between the spin current and the interfacial magnetic order should determine the SOT-driven magnetization switching in the α-Fe_2O_3/Pt bilayers. Previously, two main mechanisms have been identified as the origin of SOT:

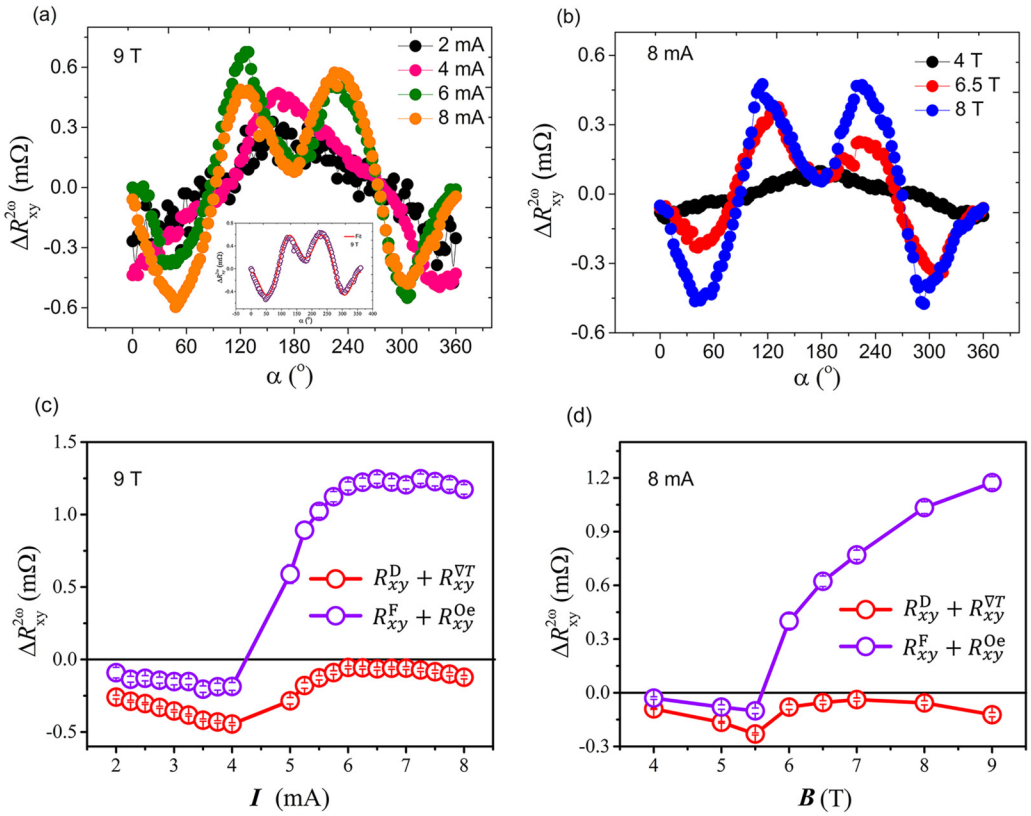

FIG. 4. (a) The transverse second-harmonic resistances ($\Delta R_{xy}^{2\omega}$) with rotating the magnetic field of 9 T on the *X*-*Y* plane with varying the amplitude of current at room temperature. The inset shows the fitted result as $I = 8$ mA. (b) The $\Delta R_{xy}^{2\omega}(\alpha)$ curves with applying AC current of 8 mA and varying in-plane magnetic field at room temperature. The extracted $R_{xy}^{D} + R_{xy}^{\nabla T}$ and $R_{xy}^{F} + R_{xy}^{Oe}$ terms as (c) varying AC current amplitude but fixed $\boldsymbol{H} = 9$ T, and (d) varying in-plane magnetic field but fixed $I = 8$ mA.

bulk or interfacial iSGE and SHE. Both torques are present in the magnetic systems lacking inversion symmetry and can provide a unique tool to manipulate the magnetic order. The iSGE-SOT, referring to the electrical generation of spin density, arises from the SOC in bulk noncentrosymmetric systems or the interfacial symmetry broken. Železný *et al.* have reported that the spin-orbit fields whose sign alternates between the spin sublattice can arise in the bulk of centrosymmetric antiferromagnets, such as Mn_2Au [19,50] and CuMnAs [51]. In this case, the efficient torque enabling the manipulation of the magnetic-order parameter is a staggered fieldlike torque [23]. In this paper, under the applied electric field ($\boldsymbol{E} = E_X \boldsymbol{X}$), the large fieldlike SOT ($\boldsymbol{T}_{FL} \sim \boldsymbol{m}_n \times \boldsymbol{S}$) in the α-Fe_2O_3/Pt bilayers indicates that the nonequilibrium distribution could lead to a large in-plane nonzero net spin density aligned perpendicular to $\boldsymbol{m}_n$ and $\boldsymbol{E}$. On the other hand, the spin current due to the bulk SHE of Pt layer should be modulated by the magnetic exchange at the interface. For small tilts of the spins from equilibrium, the Bloch equations can be expressed as $\frac{d\boldsymbol{S}}{dt} = \frac{\Delta}{\hbar}(\boldsymbol{S} \times \boldsymbol{m}_n)$, where Δ is an exchange coupling energy corresponding to exchange between the carrier spins $\boldsymbol{S}$ and $\boldsymbol{m}_n$. Furthermore, according to the semiclassical calculations by Amin and Stiles [52,53], the interfacial SOC acting on the spins passing through rather than existing in, the two-dimensional interface creates a spin polarization that couples to the magnetization through interfacial exchange interaction. Therefore, the modulated interfacial mixing conductance should also determine the change in spin absorption and reflection as a function of the magnetic vector $\boldsymbol{m}_n$. Besides, it was recently realized that the precession of spin currents around the spin-orbit field can substantially impact the SOT, which is termed the spin swapping effect [54]. Under this scenario, the primary spin current due to SHE in Pt will precess around the spin-orbit field, resulting in a secondary spin current, termed the swapping spin current. It can be absorbed by an adjacent magnetic layer, resulting in additional SOT components. Theoretically, as long as the nonmagnetic metal thickness is comparable to the mean free path, the spin swapping spin current induces a fieldlike SOT. The key ingredients in all these mechanisms are inversion-symmetry broken and the strong SOC.

In conclusion, we have investigated the SOT in the α-Fe_2O_3/Pt bilayers in which a robust interface magnetic state due to the combination of strong SOC of Pt and magnetic-field-dependent bulk magnetic order of α-Fe_2O_3 has been formed. The steplike Hall resistance variations by the pulsed current switching have been found in α-Fe_2O_3/Pt bilayers, indicating the interaction between the spin current and the interfacial magnetic vector. The sign change in the SMR with varying DC current amplitude also indicates that the magnetization at the interface can be driven by spin current. Through second-harmonic measurements, we have found that the fieldlike SOT was the dominant role and had a unique

relationship with the current intensity and the magnetic-field strength, indicating the involvement of the interfacial magnetic order.

This work was partially supported by the National Key Research and Development Program of China (Grant No. 2022YFA1402602), the National Natural Science Foundation of China (Grants No. 51971027, No. 51731003, No. 51971023, No. 51927802, No. 51971024, No. 52061135205, and No. 11905006), the Beijing Natural Science Foundation Key Program (Grant No. Z190007), and the Fundamental Research Funds for the Central Universities (Grants No. FRF-TP-19-001A3, No. FRF-MP-19-004, No. FRF-BD-20-06A, No. FRF-BD-19-010A).

[1] S. Vélez, A. Bedoya-Pinto, W. J. Yan, L. E. Hueso, and F. Casanova, Competing effects at Pt/YIG interfaces: Spin Hall magnetoresistance, magnon excitations, and magnetic frustration, Phys. Rev. B **94**, 174405 (2016).

[2] X. P. Qiu, Z. Shi, W. J. Fan, S. M. Zhou, and H. Yang, Characterization and manipulation of spin orbit torque in magnetic heterostructures, Adv. Mater. **30**, 1705699 (2018).

[3] T. Higo, K. Kondou, T. Nomoto, M. Shiga, S. Sakamoto, X. Z. Chen, D. Nishio-Hamane, R. Arita, Y. Otani, S. Miwa, and S. Nakatsuji, Perpendicular full switching of chiral antiferromagnetic order by current, Nature (London) (London) **607**, 474 (2022).

[4] B. Dieny and M. Chshiev, Perpendicular magnetic anisotropy at transition metal/oxide interfaces and applications, Rev. Mod. Phys. **89**, 025008 (2017).

[5] C.-Y. Yang, L.-C. He, Y.-S. Yen, P.-C. Chen, J.-C. Chiu, S.-D. Huang, C.-H. Tseng, and C.-H. Lai, Effect of interfacial spin configuration on y-type spin–orbit torque switching in an antiferromagnetic heavy alloy/ferromagnet bilayer, Appl. Phys. Lett. **118**, 102403 (2021).

[6] X. Z. Chen, R. Zarzuela, J. Zhang, C. Song, X. F. Zhou, G. Y. Shi, F. Li, H. A. Zhou, W. J. Jiang, F. Pan, and Y. Tserkovnyak, Antidamping-Torque-Induced Switching in Biaxial Antiferromagnetic Insulators, Phys. Rev. Lett. **120**, 207204 (2018).

[7] Y. J. Zhou, C. Y. Guo, C. H. Wan, X. Z. Chen, X. F. Zhou, R. Q. Zhang, Y. D. Gu, R. Y. Chen, H. Q. Wu, X. F. Han, F. Pan, and C. Song, Current-Induced In-Plane Magnetization Switching in a Biaxial Ferrimagnetic Insulator, Phys. Rev. Appl. **13**, 064051 (2020).

[8] A. Manchon, J. Železný, I. M. Miron, T. Jungwirth, J. Sinova, A. Thiaville, K. Garello, and P. Gambardella, Current-induced spin-orbit torques in ferromagnetic and antiferromagnetic systems, Rev. Mod. Phys. **91**, 035004 (2019).

[9] E. Cogulu, N. N. Statuto, Y. Cheng, F. Y. Yang, R. V. Chopdekar, H. Ohldag, and A. D. Kent, Direct imaging of electrical switching of antiferromagnetic Néel order in α-Fe_2O_3 epitaxial films, Phys. Rev. B **103**, L100405 (2021).

[10] R. Cheng and Q. Niu, Dynamics of antiferromagnets driven by spin current, Phys. Rev. B **89**, 081105(R) (2014).

[11] X. Z. Chen, X. F. Zhou, R. Cheng, C. Song, J. Zhang, Y. C. Wu, Y. Ba, H. B. Li, Y. M. Sun, Y. F. You, Y. G. Zhao, and F. Pan, Electric field control of Néel spin-orbit torque in an antiferromagnet, Nature Mater. **18**, 931 (2019).

[12] M. Meinert, D. Graulich, and T. Matalla-Wagner, Electrical Switching of Antiferromagnetic Mn_2Au and the Role of Thermal Activation, Phys. Rev. Appl. **9**, 064040 (2018).

[13] Y. Cheng, S. S. Yu, M. L. Zhu, J. Hwang, and F. Y. Yang, Electrical Switching of Tristate Antiferromagnetic Néel Order in $A-Fe_2O_3$ Epitaxial Films, Phys. Rev. Lett. **124**, 027202 (2020).

[14] J. Godinho, H. Reichlová, D. Kriegner, V. Novák, K. Olejník, Z. Kašpar, Z. Šobáň, P. Wadley, R. P. Campion, R. M. Otxoa, P. E. Roy, J. Železný, T. Jungwirth, and J. Wunderlich, Electrically induced and detected Néel vector reversal in a collinear antiferromagnet, Nat. Commun. **9**, 4686 (2018).

[15] M. J. Grzybowski, P. Wadley, K. W. Edmonds, R. Beardsley, V. Hills, R. P. Campion, B. L. Gallagher, J. S. Chauhan, V. Novak, T. Jungwirth, F. Maccherozzi, and S. S. Dhesi, Imaging Current-Induced Switching of Antiferromagnetic Domains in CuMnAs, Phys. Rev. Lett. **118**, 057701 (2017).

[16] S. Fukami, C. L. Zhang, S. DuttaGupta, A. Kurenkov, and H. Ohno, Magnetization switching by spin-orbit torque in an antiferromagnet-ferromagnet bilayer system, Nature Mater. **15**, 535 (2016).

[17] S. Arpaci, V. Lopez-Dominguez, J. C. Shi, L. Sánchez-Tejerina, F. Garesci, C. L. Wang, X. T. Yan, V. K. Sangwan, M. A. Grayson, M. C. Hersam, G. Finocchio, and P. K. Amiri, Observation of current-induced switching in non-collinear antiferromagnetic $IrMn_3$ by differential voltage measurements, Nat. Commun. **12**, 3828 (2021).

[18] P. X. Zhang, J. Finley, T. Safi, and L. Q. Liu, Quantitative Study on Current-Induced Effect in an Antiferromagnet Insulator/Pt Bilayer Film, Phys. Rev. Lett. **123**, 247206 (2019).

[19] J. Železný, H. Gao, K. Výborný, J. Zemen, J. Mašek, A. Manchon, J. Wunderlich, J. Sinova, and T. Jungwirth, Relativistic Néel-order Fields Induced by Electrical Current in Antiferromagnets, Phys. Rev. Lett. **113**, 157201 (2014).

[20] K. Wang, L. J. Qian, S.-C. Ying, and G. Xiao, Spin-orbit torque switching of chiral magnetization across a synthetic antiferromagnet, Commun. Phys. **4**, 10 (2021).

[21] J. Sinova, S. O. Valenzuela, J. Wunderlich, C. H. Back, and T. Jungwirth, Spin Hall effects, Rev. Mod. Phys. **87**, 1213 (2015).

[22] I. Garate and M. Franz, Inverse Spin-Galvanic Effect in the Interface between a Topological Insulator and a Ferromagnet, Phys. Rev. Lett. **104**, 146802 (2010).

[23] V. Baltz, A. Manchon, M. Tsoi, T. Moriyama, T. Ono, and Y. Tserkovnyak, Antiferromagnetic spintronics, Rev. Mod. Phys. **90**, 015005 (2018).

[24] R. Ivantsov, O. Ivanova, S. Zharkov, M. Molokeev, A. Krylov, I. Gudim, and I. Edelman, Magnetic circular dichroism in the canted antiferromagnet α-Fe_2O_3: Bulk single crystal and nanocrystals, J. Magn. Magn. Mater. **498**, 166208 (2020).

[25] J. H. Han, P. X. Zhang, Z. Bi, Y. B. Fan, T. S. Safi, J. X. Xiang, J. Finley, L. Fu, R. Cheng, and L. Q. Liu, Birefringence-like spin transport via linearly polarized antiferromagnetic magnons, Nat. Nanotechnol. **15**, 563 (2020).

[26] N. Shimomura, S. P. Pati, Y. Sato, T. Nozaki, T. Shibata, K. Mibu, and M. Sahashi, Morin transition temperature in (0001)-

oriented α-Fe_2O_3 thin film and effect of Ir doping, J. Appl. Phys. **117**, 17c736 (2015).

[27] J. Miyawaki, S. Suga, H. Fujiwara, M. Urasaki, H. Ikeno, H. Niwa, and H. Kiuchi, and Y. Harada, Dzyaloshinskii-Moriya interaction in $\alpha-Fe_2O_3$ measured by magnetic circular dichroism in resonant inelastic soft x-ray scattering, Phys. Rev. B **96**, 214420 (2017).

[28] T. Z. Zhang, K. K. Meng, X. Shi, Y. B. Deng, L. B. Zhu, X. G. Xu, and Y. Jiang, Spin Hall magnetoresistance in antiferromagnetic α-Fe_2O_3/Pt bilayers: Modulation from interface magnetic state, Appl. Phys. Lett. **121**, 262404 (2022).

[29] See Supplemental Material at http://link.aps.org/supplemental/10.1103/PhysRevB.108.014422 for a more detailed discussion.

[30] R. Lebrun, A. Ross, S. A. Bender, A. Qaiumzadeh, L. Baldrati, J. Cramer, A. Brataas, R. A. Duine, and M. Kläui, Tunable long-distance spin transport in a crystalline antiferromagnetic iron oxide, Nature **561**, 222 (2018).

[31] S. Y. Bodnar, L. Šmejkal, I. Turek, T. Jungwirth, O. Gomonay, J. Sinova, A. A. Sapozhnik, H.-J. Elmers, M. Kläui, and M. Jourdan, Writing and reading antiferromagnetic Mn_2Au by Néel spin-orbit torques and large anisotropic magnetoresistance, Nat. Commun. **9**, 348 (2018).

[32] S. R. Boona, R. C. Myers, and J. P. Heremans, Spin caloritronics, Energy Environ. Sci. **7**, 885 (2014).

[33] B. L. Zink, Thermal effects in spintronic materials and devices: An experimentalist's guide, J. Magn. Magn. Mater. **564**, 170120 (2022).

[34] C. H. Back, G. E. W. Bauer, and B. L. Zink, Special issue on spin caloritronics, J. Phys. D: Appl. Phys. **52**, 230301 (2019).

[35] G. E. W. Bauer, E. Saitoh, and B. J. van Wees, and Spin caloritronics, Nature Mater. **11**, 391 (2012).

[36] Y. Cheng, S. S. Yu, A. S. Ahmed, M. L. Zhu, Y. Rao, M. Ghazisaeidi, J. Hwang, and F. Y. Yang, Anisotropic magnetoresistance and nontrivial spin Hall magnetoresistance in Pt/$\alpha-Fe_2O_3$ bilayers, Phys. Rev. B **100**, 220408(R) (2019).

[37] C. C. Chiang, S. Y. Huang, D. Qu, P. H. Wu, and C. L. Chien, Absence of Evidence of Electrical Switching of the Antiferromagnetic Néel Vector, Phys. Rev. Lett. **123**, 227203 (2019).

[38] P. X. Zhang, C.-T. Chou, H. Yun, B. C. McGoldrick, J. T. Hou, K. A. Mkhoyan, and L. Q. Liu, Control of Néel Vector with Spin-Orbit Torques in an Antiferromagnetic Insulator with Tilted Easy Plane, Phys. Rev. Lett. **129**, 017203 (2022).

[39] C. O. Avci, K. Garello, A. Ghosh, M. Gabureac, S. F. Alvarado, and P. Gambardella, Unidirectional spin Hall magnetoresistance in ferromagnet/normal metal bilayers, Nat. Phys. **11**, 570 (2015).

[40] Y. Lv, J. Kally, D. L. Zhang, J. S. Lee, M. Jamali, N. Samarth, and J.-P. Wang, Unidirectional spin-Hall and Rashba-Edelstein magnetoresistance in topological insulator-ferromagnet layer heterostructures, Nat. Commun. **9**, 111 (2018).

[41] J. Lustikova, Y. Shiomi, N. Yokoi, N. Kabeya, N. Kimura, K. Ienaga, S. Kaneko, S. Okuma, S. Takahashi, and E. Saitoh, Vortex rectenna powered by environmental fluctuations, Nat. Commun. **9**, 4922 (2018).

[42] P. He, S. S.-L. Zhang, D. P. Zhu, Y. Liu, Y. Wang, J. W. Yu, G. Vignale, and H. Yang, Bilinear magnetoelectric resistance as a probe of three-dimensional spin texture in topological surface states, Nat. Phys. **14**, 495 (2018).

[43] T. Ideue, K. Hamamoto, S. Koshikawa, M. Ezawa, S. Shimizu, Y. Kaneko, Y. Tokura, N. Nagaosa, and Y. Iwasa, Bulk rectification effect in a polar semiconductor, Nat. Phys. **13**, 578 (2017).

[44] T. Yokouchi, N. Kanazawa, A. Kikkawa, D. Morikawa, K. Shibata, T. Arima, Y. Taguchi, F. Kagawa, and Y. Tokura, Electrical magnetochiral effect induced by chiral spin fluctuations, Nat. Commun. **8**, 866 (2017).

[45] R. Ramos, T. Kikkawa, A. Anadón, I. Lucas, T. Niizeki, K. Uchida, P. A. Algarabel, L. Morellón, M. H. Aguirre, M. R. Ibarra, and E. Saitoh, Interface-induced anomalous Nernst effect in Fe_3O_4/Pt-based heterostructures, Appl. Phys. Lett. **114**, 113902 (2019).

[46] S. Geprags, A. Kehlberger, F. D. Coletta, Z. Y. Qiu, E.-J. Guo, T. Schulz, C. Mix, S. Meyer, A. Kamra, M. Althammer, H. Huebl, G. Jakob, Y. Ohnuma, H. Adachi, J. Barker, S. Maekawa, G. E. W. Bauer, E. Saitoh, R. Gross, S. T. B. Goennenwein, and M. Kläui, Origin of the spin Seebeck effect in compensated ferrimagnets, Nat. Commun. **7**, 10452 (2016).

[47] S. M. Wu, W. Zhang, A. KC, P. Borisov, J. E. Pearson, J. S. Jiang, D. Lederman, A. Hoffmann, and A. Bhattacharya, Antiferromagnetic Spin Seebeck Effect, Phys. Rev. Lett. **116**, 097204 (2016).

[48] S. Maeka, S. O. Valenzuela, E. Saitoh, and T. Kimura, *Spin current*, 1st ed., edited by S. Maeka, S. O. Valenzuela, E. Saitoh, and T. Kimur (Oxford University Press, Oxford, UK, 2012).

[49] S. Onoda, N. Sugimoto, and N. Nagaosa, Quantum transport theory of anomalous electric, thermoelectric, and thermal Hall effects in ferromagnets, Phys. Rev. B **77**, 165103 (2008).

[50] J. Železný, H. Gao, A. Manchon, F. Freimuth, Y. Mokrousov, J. Zemen, J. Mašek, J. Sinova, and T. Jungwirth, Spin-orbit torques in locally and globally noncentrosymmetric crystals: Antiferromagnets and ferromagnets, Phys. Rev. B **95**, 014403 (2017).

[51] P. Wadley, V. Hills, M. R. Shahedkhah, K. W. Edmonds, R. P. Campion, V. Novák, B. Ouladdiaf, D. Khalyavin, S. Langridge, V. Saidl, P. Nemec, A. W. Rushforth, B. L. Gallagher, S. S. Dhesi, F. Maccherozzi, J. Železný, and T. Jungwirth, Antiferromagnetic structure in tetragonal CuMnAs thin films, Sci. Rep. **5**, 17079 (2015).

[52] V. P. Amin and M. D. Stiles, Spin transport at interfaces with spin-orbit coupling: Formalism, Phys. Rev. B **94**, 104419 (2016).

[53] V. P. Amin and M. D. Stiles, Spin transport at interfaces with spin-orbit coupling: Phenomenology, Phys. Rev. B **94**, 104420 (2016).

[54] H. B. M. Saidaoui and A. Manchon, Spin-Swapping Transport and Torques in Ultrathin Magnetic Bilayers, Phys. Rev. Lett. **117**, 036601 (2016).